

Density-functional study of plutonium monoxide monohydride

Ruizhi Qiu^a, Haiyan Lu^a, Bingyun Ao^a, Tao Tang^a, Piheng Chen^a

^a*Science and Technology on Surface Physics and Chemistry Laboratory, Mianyang 621908, Sichuan, P.R. China*

Abstract

The structural, electronic, mechanical, optical, thermodynamic properties of plutonium monoxide monohydride (PuOH) are studied by density-functional calculations within the framework of LDA/GGA and LDA/GGA+ U . From the total energy calculation, the lowest-energy crystal structure of PuOH is predicted to have space group $F\bar{4}3m$ (No. 216). Within the LDA+ U framework, the calculated lattice parameter of $F\bar{4}3m$ -PuOH is in good agreement with the experimental value and the corresponding ground state is predicted to be an antiferromagnetic charge-transfer insulator. Furthermore, we investigate the bonding character of PuOH by analyzing the electron structure and find that there are a stronger Pu-O bond and a weaker Pu-H bond. The mechanical properties including the elastic constants, elastic moduli and Debye's temperature, and the optical properties including the reflectivity and absorption coefficient are also calculated. We then compute the phonon spectrum which verified the dynamical stability of $F\bar{4}3m$ -PuOH. Some thermodynamic quantities such as the specific heat are evaluated. Finally we calculate the formation energy of PuOH, and the reaction energies for the oxidation of PuOH and PuOH-coated Pu, which are in reasonable agreement with the experimental values.

Keywords: PuOH, density functional theory, crystal structure, reaction energy

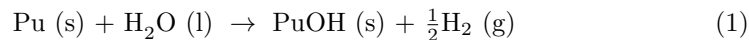
*Corresponding author

Email addresses: qiuruizhi@itp.ac.cn (Ruizhi Qiu), chenph@live.cn (Piheng Chen)

1. Introduction

The corrosion of plutonium have been attracting considerable interest in surface chemistry, corrosion chemistry and condensed matter physics [1–9]. In addition, it is also an important issue for handling and storage of this chemically active and radioactive material [4, 10]. Of considerable concern is the corrosion products which are formed by reaction of plutonium with water, air and hydrogen [4, 11–18]. These corrosion products, such as Pu_2O_3 and PuH_x , were suggested to promote the corrosion of metal.

Plutonium monoxide monohydride (PuOH) is a potentially reactive compound formed by corrosion of Pu in liquid water or moisture at room temperature [13–16]. In particular, PuOH is considered to initiate the rapid hydride-catalyzed corrosion of PuOH -coated plutonium metals [4, 17], and identified as a key product to understand the chloride-catalyzed corrosion of plutonium in glovebox atmospheres [18]. The following equation



describes the formation of PuOH in near-neutral water and also determines the composition of the product from experimental data showing that 0.5 mol of H_2 is formed by the reaction of 1.0 mol of Pu. The identification of PuOH is also based on the thermal gravity (TG), X-ray photoelectron spectroscopy (XPS) and X-ray diffraction (XRD) analyses [14]. From the XRD analysis, PuOH has a CaF_2 -related structure formed by a cationic sublattice of Pu (III) and an anionic sublattice of O^{2-} and H^- . However, the specific arrangement of O and H atoms is unknown, which may be ascribed to the small scattering cross section of these light atoms with respect to the heavy Pu atom. This structural uncertainties have impeded in-depth understanding and further exploration of PuOH .

Moreover, there are very limited experimental reports of the basic properties of PuOH , which may be attributed to the difficulties in preparing and handling samples. Besides the above-mentioned partially-determined structure,

only the thermodynamic properties about the formation enthalpies of PuOH,
30 the reactions of PuOH and PuOH-coated Pu with O₂ are estimated [17]. In
fact, density-functional study has already been performed to deeply understand
the basic properties of plutonium metal, oxides and hydrides [19–29]. Therefore
it is interesting and necessary to perform the density functional theory (DFT)
calculations to systematically investigate the ground state properties of PuOH,
35 including the prediction of the Wyckoff positions of O and H.

In this work, we have predicted the ground state crystal structure from the
perspective of the energetic stability, and systematically calculate the electronic,
optical, mechanical and thermodynamic properties of PuOH. The rest of this pa-
per is organized as follows. The computational details are described in section 2,
40 and the results are presented and discussed in section 3. Section 4 presents a
brief summary.

2. Computational details

This study was performed using the VASP code [30]. The projector aug-
mented wave (PAW) [31, 32] pseudopotentials for Pu, O, and H with the
45 $6s^26p^26d^25f^4$, $2s^22p^2$, and $1s^1$ valence electronic configurations are chosen.
For the exchange and correlation energy, both the local density approximation
(LDA) [33] and the generalized gradient approximation (GGA) using Perdew-
Becke-Ernzerhof (PBE) [34] functional are employed. In addition, we also stud-
ied three possibilities for the magnetic states: nonmagnetic (NM), antiferromag-
50 netic (AFM), ferromagnetic (FM). The kinetic energy cutoff is taken as 700 eV
and an $8 \times 8 \times 8$ Monkhorst-Pack k point sampling mesh [35] of Brillouin zone
is used.

In order to capture the localization effect of the f electrons coming from
the strong electron-electron interaction, we employed the so-called DFT+ U ap-
55 proach which has been successfully applied to δ -plutonium [19], plutonium ox-
ides [20–23] and hydrides [24–29]. Here we choose the rotationally invariant
DFT+ U scheme introduced by Liechtenstein *et. al.* [36], which was already

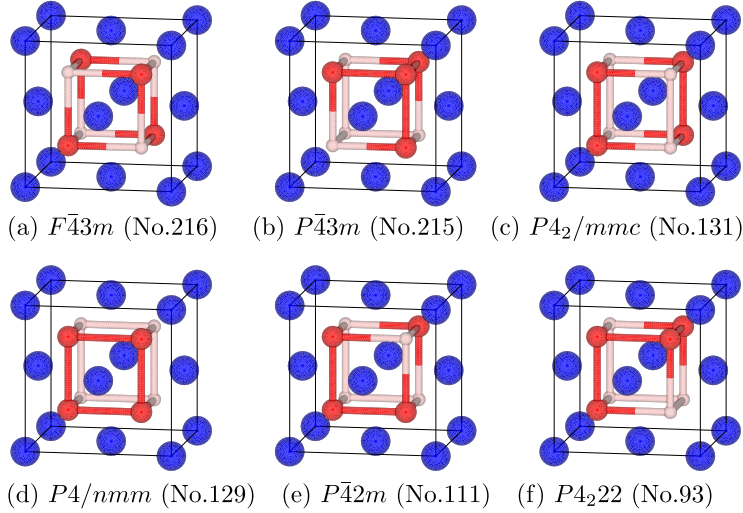


Figure 1: Six possible fluorite-related crystal structures of PuOH with the blue, red, pink balls representing Pu, O, H atoms, respectively.

adopt in the study of Pu [19] and PuO₂ [21]. Unless otherwise stated, the typical set of parameters: $U=4.0$ eV and $J=0.7$ eV, are chosen in the following.

60 3. Results and discussion

3.1. Crystal structure

As concerns the fluorite-related structures of PuOH, Pu occupied the positions in an face-centered cubic (fcc) configuration while O or H occupied the eight tetrahedral sites of the fcc lattice. In order to consider all the possible ar-
65 rangement, one can randomly select four tetrahedral sites to accommodate the H atoms and the residual tetrahedral sites for the O atoms. After symmetry analyses, one can found that there are only six inequivalent atomic configurations, which are shown in Figure 1. The space groups include $F\bar{4}3m$, $P\bar{4}3m$, $P4_2/mmc$, $P4/nmm$, $P\bar{4}2m$ and $P4_222$, which would be used to denote the
70 crystal structures below.

For $F\bar{4}3m$ phase (Figure 1 (a)), four hydrogen atoms are fully separated from each other and the corresponding symmetry is the highest. For the structure

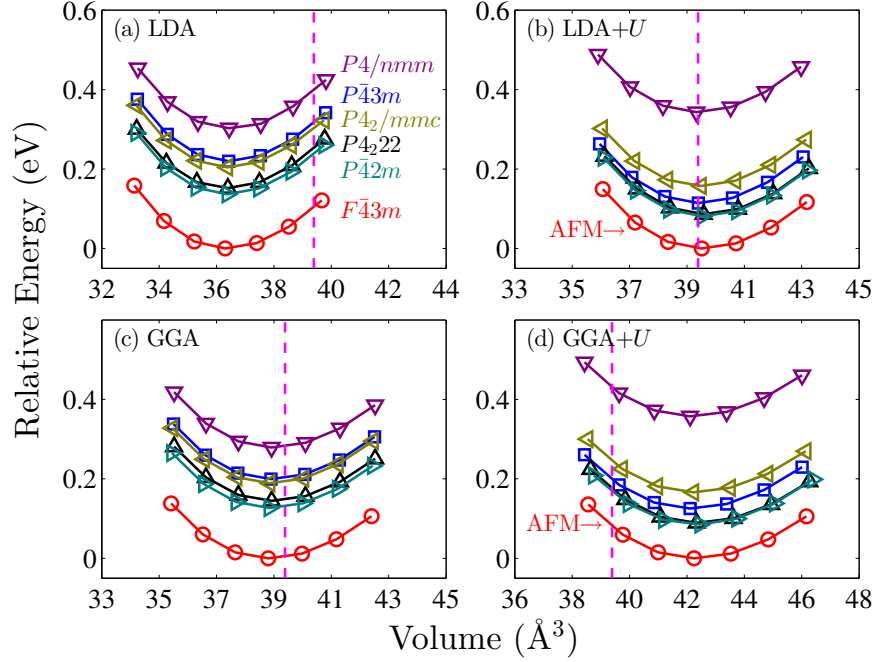


Figure 2: Calculated total energies for the six fluorite-related structures of PuOH as a function of volume within four exchange-correlation functional approximations: (a) LDA, (b) LDA+U, (c) GGA, and (d) GGA+U. The dashed lines denote the experimental volume. All the magnetic states presented here are FM except AFM $F\bar{4}3m$ -phase in the LDA/GGA+U scheme, denoted as the bottom lines in (b) and (d).

with the second highest symmetry, $P\bar{4}3m$ phase (Figure 1 (b)), four hydrogen atoms are connected to each other and constitute a trirectangular tetrahedron.

75 For $P4_2/mmc$ and $P4/nmm$ phase (Figure 1 (c) and (d)), four hydrogen atoms are located in the $\{110\}$ and $\{100\}$ plane, respectively. For $P\bar{4}2m$ phase (Figure 1 (e)), three hydrogen atoms constitute a right-angle and the fourth hydrogen atom is located away from them. For the structure with lowest symmetry, $P4_222$ phase (Figure 1 (f)), four hydrogen atoms constitute two right angles.

80 If the O-H system in the central region of the fcc lattice is viewed as the O-H mixture, the $F\bar{4}3m$ mixture is the most homogeneous and the segregation of the $P4/nmm$ and $P\bar{4}3m$ mixtures are the most serious.

Total energies for the six possible fluorite-related structures of PuOH are calculated within density functional theory as a function of lattice constant. For each space group, the total energies are obtained using three magnetic orders (NM, AFM, and FM) and only the lowest one of the three is presented. In Figure 2, the total energy for all phases are plotted as a function of volume. Here and in the following the values of energy and volume are presented per formula unit. Notice first that our calculation shows that the $F\bar{4}3m$ phase is the most stable whatever the exchange-correlation functional approximation we choose. Besides, all the relative energies of the other phases are greater than 81 meV (equivalent to 940 K), which implies that PuOH would only adopt the space group $F\bar{4}3m$ (Figure 1 (a)) in the room temperature or intermediate temperature.

Furthermore, the energetics stability ordering of the six fluorite-related structures can also be obtained from Figure 2, which is $F\bar{4}3m < P\bar{4}2m < P4_2/mmc < P4_222 < P\bar{4}3m < P4/nmm$ for LDA/GGA, and $F\bar{4}3m < P\bar{4}2m < P4_2/mmc < P\bar{4}3m < P4_222 < P4/nmm$ for LDA/GGA+ U . Recalling of the above analogy of the structure with the O-H mixture, we realized that the system is more stable for lower degree of segregation. The statement might be universal for various Pu+O+H systems, which signifies that the stability of the system may be achieved for the homogeneous O-H mixture and hydrogen transport may be rapid for the low-oxygen system.

3.2. Structural properties

Now let us focus on the $F\bar{4}3m$ phase. In this cubic unit cell defined by lattice parameter a_0 , the crystallographic positions are Pu $4a$ (0,0,0), H $4c$ ($\frac{1}{4}, \frac{1}{4}, \frac{1}{4}$), and O $4d$ ($\frac{3}{4}, \frac{3}{4}, \frac{3}{4}$) (or H $4d$ and O $4c$). Since the NM phase of PuOH is not energetically favorable compared with their FM and AFM phases, we will concentrate on the phases with magnetic order. The magnetic states predicted by our LDA/GGA calculation is FM while that from the LDA/GGA+ U calculation is AFM. To display the FM-AFM transition, we show in Figure 3 (a) the dependence of $E_{\text{FM}} - E_{\text{AFM}}$ on the Hubbard parameter U . For LDA+ U , the

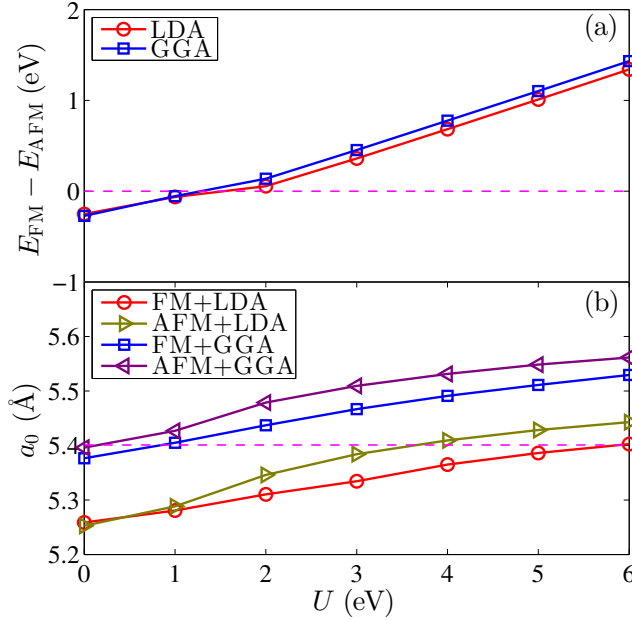


Figure 3: Dependence of (a) energy difference between AFM and FM order and (b) equilibrium lattice parameter on Hubbard parameter U . The dashed line labels the transition and the experimental lattice parameter in (a) and (b), respectively. Note that $U = 0$ means pure LDA/GGA rather than LDA/GGA+ U with $U = 0$.

total energy of the AFM phase is lower than of the FM phase for U larger than ~ 1.4 eV, while for GGA+ U , the turning point occurs at a small U of ~ 1.2 eV. The total energy differences $E_{\text{AFM}} - E_{\text{FM}}$ within the LDA+ U and GGA+ U at $U=4$ eV are 0.68 and 0.78 eV, respectively. This large value of energy difference suggests that the $F\bar{4}3m$ phase of PuOH is AFM.

Now let us focus on the lattice parameter a_0 . In Figure 3 (b) we plot the dependence of a_0 on U . The values of a_0 are obtained by fitting the energy-volume data with the third-order Birch-Murnaghan equation of state (EOS) fitting [38]. The EOS fitting also yields the equilibrium volume V_0 and bulk modulus B as follows. Similar to the study of PuO₂ and PuH₂ [20, 21, 24], the Hubbard U correction in the LDA/GGA+ U approach leads to an increase of the equilibrium lattice parameter.

125 Both the pure LDA and GGA underestimated the lattice parameter of FM
and AFM PuOH, as clearly shown in Figure 3 (b). At a typical value of $U = 4$
eV, result of AFM phase within the LDA+ U formalism (5.409 Å) is in close
agreement with the experimental value (5.401 Å). Therefore it is suitable for us
to focus on the results obtained for $U = 4.0$ eV, which we assumed to be the
130 reference value for PuOH and also chosen in the study of Pu [19] and PuO₂ [21].

In Table 1, we listed a_0 , V_0 , B , pressure derivative of the bulk modulus
 B' , band gap Δ and magnetic moment of Pu atom μ_{mag} in the framework of
LDA/GGA and LDA/GGA+ U . Clearly, our calculations predicted that PuOH
is an AFM insulator, which is similar to PuO₂.

135 It is interesting to compare the structure properties of PuOH with that of
PuO₂ [21] and PuH₂ [28] with the same fluorite-related structure. It is intuitive
to regard that there is a monotonic evolution along PuO₂ \rightarrow PuOH \rightarrow PuH₂.
So it is with the bulk modulus B and energy gap Δ . But for the lattice param-
eters, the value of PuOH in the LDA/GGA+ U formalism is greater than that of
140 PuO₂ (5.338/5.444 Å [21]) and PuH₂ (5.337/5.418 Å [28]). Actually, the exper-
imental values of these compounds have already confirmed this point, although
the difference is much smaller. In order to understanding this non-monotonic
evolution, it is necessary to discuss the corresponding electronic structure in
section 3.4.

145 3.3. Mechanical properties

The mechanical properties, by which we understand the behavior of materials
under external forces, are of special importance in fabrication processes and
applications. The mechanical properties of a crystal are described by considering
this crystal as a homogeneous continuum medium, i.e., an elastic body, rather
150 than a periodic array of atoms. For an elastic body, the Hooke's law holds
and the corresponding elastic properties are total determined by the elastic
tensor, which is the coefficient that relates the stress to the strain. In our
work, the elastic tensor is also derived from the strain-stress relationship [39]
by performing finite distortions of the lattice and also allowing the internal

Table 1: Equilibrium properties of $F\bar{4}3m$ -PuOH. The lattice parameters a_0 , volume V_0 , bulk modulus B , and pressure derivative of the bulk modulus B' , band gap Δ , and magnetic moment of Pu atom μ_{mag} are reported for LDA, GGA, LDA+ U , and GGA+ U . Experimental values are also shown for comparison.

Properties	LDA	GGA	LDA+ U	GGA+ U	Exp.
a_0 (Å)	5.259	5.377	5.409	5.531	5.401 [14]
V_0 (Å ³)	36.35	38.85	39.57	42.31	39.39
B_0 (GPa)	150	123	131	111	
B'	4.4	4.4	4.1	4.1	
Δ (eV)	0.0	0.0	1.298	1.683	
μ_{mag} (μ_B)	4.901	4.948	4.984	5.027	

155 relaxation of the ions. For the elastic tensor of a cubic crystal, there are only three independent elastic constants, i.e., c_{11} , c_{12} , and c_{44} .

For polycrystal, the mechanical properties are evaluated by the elastic moduli, including bulk modulus B , shear modulus G , Young's modulus E , and Poisson's ratio ν , which are the measure of the compressibility, rigidity, stiffness, and Poisson's effect, respectively. The polycrystalline elastic moduli could be calculated by employing the Voigt-Reuss-Hill approximation [40]. In this approach, the effective moduli are approximated by the arithmetic mean of the two well-known bounds for monocrystals according to Voigt [41] and Reuss and Agnew [42]. For a cubic system, the mathematical formulation is provided in the following equations [40]:

$$B = \frac{c_{11} + 2c_{12}}{3}, \quad (2)$$

$$G = \frac{1}{2} \left(\frac{c_{11} - c_{12} + 3c_{44}}{5} + \frac{5c_{44}(c_{11} - c_{12})}{4c_{44} + 3(c_{11} - c_{12})} \right), \quad (3)$$

$$E = \frac{9BG}{3B + G}, \quad (4)$$

$$\nu = \frac{3B - E}{6B}. \quad (5)$$

In Debye's theory [43, 44], the solid was also treated as the elastic body,

and the lattice vibrations are regarded as the elastic waves. In order to im-
 pose a finite number of modes in the solid, Debye used a maximum allowed
 frequency ω_D , i.e., the frequency of the highest normal mode of vibration. The
 170 corresponding temperature is the so-called Debye temperature, $\theta_D = h\omega_D/k_B$
 with h and k_B being the Planck and Boltzmann constants, respectively. Now
 the Debye temperature θ_D becomes one of the simplest and the most useful
 parameters to understand thermodynamics properties of solid. In addition, θ_D
 is also a measure of the hardness of the solid [45].

175 The same elastic assumptions imply that θ_D could be evaluated in terms of
 the elastic moduli. The relation between the Debye temperature θ_D with elastic
 moduli is given by

$$\theta_D = \frac{h}{k_B} \left[\frac{9n}{4\pi V_0} \right]^{1/3} \left[2 \left(\frac{\rho}{G} \right)^{3/2} + \left(\frac{3\rho}{3B + 4G} \right)^{3/2} \right]^{-1/3}, \quad (6)$$

in which n is the number of atoms in one formula and ρ is the mass density.

In Table 2 we listed the calculated elastic constants, elastic moduli, Poisson's
 180 ratio, and Debye temperature of $F\bar{4}3m$ -PuOH. Notice that the bulk modulus B
 deduced from elastic constants are very close to that obtained by EOS fitting
 in Table 1. This indicates that our calculations are consistent and reliable.

Let us focus on the mechanical stability first. For cubic crystals, the stability
 criteria requires that

$$c_{44} > 0, \quad c_{11} > c_{12}, \quad c_{11} + 2c_{12} > 0, \quad (7)$$

185 which implies that the energy change upon any small deformation is positive.
 Obviously, the $F\bar{4}3m$ phase of PuOH is mechanically stable.

Moreover, let us note that the Hubbard U correction in the LDA/GGA+ U
 approach leads to a decrease of the elastic constants and elastic moduli. As
 was the case of PuO₂ [22]. Next let us compare the mechanical properties of
 190 PuOH with that of PuO₂ [22] with the same fluorite-related structure. Take
 the results from LDA+ U framework as an example (c_{11} =319.6 GPa, c_{12} =177.8
 GPa, c_{44} =74.5 GPa for PuO₂ [22]). The values of c_{11} and c_{12} of PuOH are up

to 50% smaller than that of PuO₂, while the value of c_{44} of PuOH is almost the same as that of PuO₂. This signifies that PuOH is sensitive to compress strain and insensitive to shear strain compare to PuO₂. This point is also confirmed by comparing the values of elastic moduli.

Table 2: Mechanical properties of $F\bar{4}3m$ -PuOH. The elastic constants (C_{11} , C_{12} , C_{44}), bulk modulus (B), Shear modulus (G), Young’s modulus (E), Possion’s ratio (ν), Debye’s temperature (θ_D) are reported for LDA, GGA, LDA+ U , and GGA+ U .

Method	C_{11} (GPa)	C_{12} (GPa)	C_{44} (GPa)	B (GPa)	G (GPa)	E (GPa)	ν	θ_D (K)
LDA	221	115	79	150	67	176	0.31	344
GGA	194	88	72	123	64	163	0.28	337
LDA+ U	198	96	77	130	65	168	0.28	343
GGA+ U	182	73	64	109	60	152	0.27	332

3.4. Electronic structure

The vast array of electrical, optical and magnetic properties of the material are determined by the electronic structure. In Figure 4 we plot the total density of states (DOS) as well as the projected DOS for the Pu $5f$, Pu $6d$ O $2p$, H $1s$ orbitals of PuOH within the LDA and LDA+ U formalisms. Results from GGA and GGA+ U are similar and hence are not shown here. Obviously, The ground state of $F\bar{4}3m$ -PuOH is predicted to be metallic for the pure LDA and insulating for LDA+ U , which is similar to PuO₂ [20–22]. Based on the ubiquitous localized nature of $5f$ electron in Pu compound and the above discussion in section 3.2, we conclude that PuOH is an antiferromagnetic insulator with space group $F\bar{4}3m$.

From the partial DOS (pDOS), $F\bar{4}3m$ -PuOH is predicted to be a charge-transfer insulator from the pDOS in Figure 4. This behavior is similar to PuO₂ [46, 47], but not Pu₂O₃ which has the same formal charge with PuOH. Below the Fermi level, the shape of O- $2p$ pDOS follows that of Pu- $5f$ pDOS, especially for the peak around -2 eV. These indicate the probable presence of

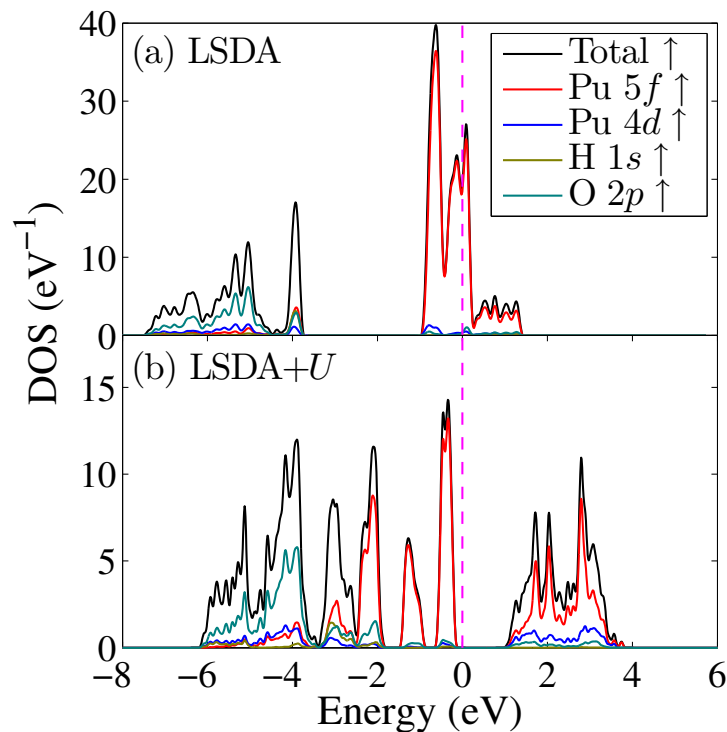


Figure 4: The total DOS for the PuOH computed in the (a) LDA, (b) LDA+ U ($U=4$) formalisms. The projected DOSs for the Pu 5*f*, Pu 6*d*, O 2*p*, and H 1*s* orbitals are also shown. The Fermi level is set at zero and labeled by the dashed line.

Pu-O covalent bond. In order to clarify the bonding character in PuOH, we present in Figure 5 the charge-density distribution of (110) plane calculated in LDA+ U formalism. For one Pu atom, there are two nearest-neighboring H atoms and two nearest-neighboring O atoms in one (110) plane, as illustrated in Figure 5. The charge density distribution around O and H atoms are nearly circular with slight deformation toward Pu atoms. And the charge density distribution around Pu atom are significantly deformed toward O atoms, forming a square-like shape due to the T_d point group of 4*a* Wyckoff position. The covalent bridges between Pu and O atoms are clear and there is also visible bridges between Pu and H atoms. Thus we draw the conclusion that the Pu-O

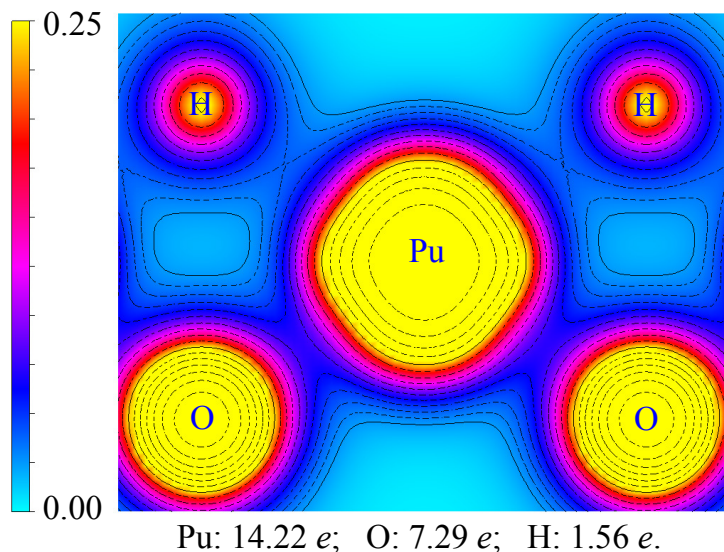


Figure 5: A slice of the isosurfaces of the electron density in the (110) plane from the LDA+ U calculation. The bottom list the total valence electron charge for Pu, O, and H atoms according to Bader’s partitioning.

bond is stronger than the Pu-H bond in this system. Since there is a blank area between H and O atoms and their distance is as large as 2.7 \AA ($a_0/2$), we can deduce that there is no H-O bond in this system and PuOH is not an alkali. This conclusion agrees with the experimental observation that PuOH is insoluble in near-neutral water [16].

To understand the ionicity of PuOH, we carry out the Bader’s charge analysis [48] and the results are listed in the bottom of Figure 4. The charge value of O atom in PuOH is closed to that in PuO₂ (7.20 e) [22], and the charge value of H atom is close to that in PuH₃ (1.50 e) [28]. These observations manifest that the formal charges of O and H could be regarded as O²⁻ and H⁻, respectively. In addition, the charge of Pu atom in PuOH is lower than that that in PuO₂ (13.60 e) [22] but larger than that in PuH₃ (14.58 e) [28], which indicates the lower valence state of Pu atom (Pu III). The results are consistent with the experimental argument [16].

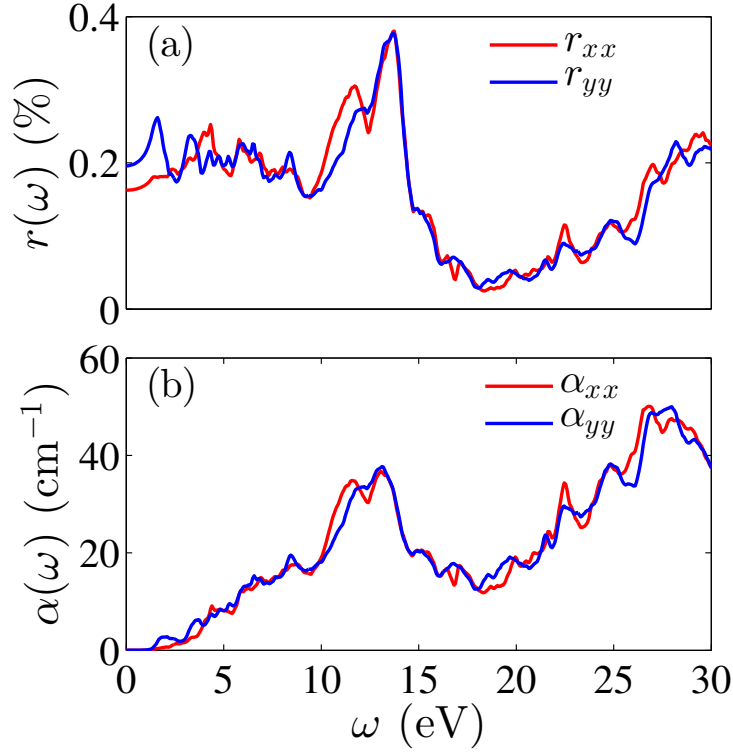


Figure 6: (a) The reflectivity and (b) absorption coefficient of PuOH along two directions.

3.5. Optical properties

Due to the radioactivity of plutonium compounds, contactless identification of various materials is very necessary, and obviously one of the useful tools is optical detection. Thus understanding the optical properties of PuOH is extremely important. Experimental data are not available now.

The optical properties as well as the electrical conductivity are determined by the frequency-dependent dielectric function $\epsilon(\omega)$, which has both real and imaginary parts: $\epsilon(\omega) = \epsilon_1(\omega) + i\epsilon_2(\omega)$. The dielectric function $\epsilon(\omega)$ is determined from the Kubo-Greenwood formula [49, 50] within the independent-particle approximation. The technical details are described in Ref. [51]. The real (n) and imaginary (k) parts of the index of refraction are related to the dielectric

function by a simply formula:

$$\epsilon(\omega) = \epsilon_1(\omega) + i\epsilon_2(\omega) = [n(\omega) + ik(\omega)]^2. \quad (8)$$

The index of refraction defines the reflectivity (r) and absorption coefficient (α):

$$r(\omega) = \frac{[1 - n(\omega)]^2 + [k(\omega)]^2}{[1 + n(\omega)]^2 + [k(\omega)]^2}, \quad \alpha(\omega) = 2\omega k(\omega). \quad (9)$$

The reflectivity and absorption coefficients of PuOH are plotted in Figure 6. Due to the presence of AFM, the optical properties along the direction of the magnetic moment (x in our study) is slightly different from that perpendicular to the direction of magnetic moment (y and z in our study). The main difference lies in the first peak of $r_{yy}(\omega)$ in Figure 6 (a) at 1.6 eV, which is contributed by the transition from the top of valence bands to the bottom of conduction bands in Figure 4. This transition also contributes to the rising of the absorption coefficients. Two main peaks are observed at 11.7 eV and 13 eV, which mainly contributed by the transition to higher energy levels. Reflectivity of PuOH at $\omega = 0$ is not far from the value obtained for PuO₂ [21, 52].

3.6. Thermodynamical properties

All the above discussions are about zero-temperature, but the state of a physical system is usually relevant to the finite temperature T . From this perspective, it is of great importance to understand the thermodynamical properties of PuOH. Usually, the thermodynamical properties are easily measurable and for PuOH, some thermodynamical quantities are already estimated in Ref. [17].

Thermodynamic properties of crystals are mainly determined by lattice vibrations, i.e., the phonons. Using the PHONOPY code [53], the phonon frequencies are computed from the real-space force constants. And the force constants are calculated in the density-functional perturbation theory (DFPT) within the LDA+ U scheme. In Figure 7 we plot the phonon spectrum along K - Γ - X - Γ - L directions in the Brillouin Zone (BZ) and also the phonon density of states (PDOS). In the spectrum, there are totally nine phonon modes attributed to the three atoms in the primitive cell. Due to the mass difference among Pu,

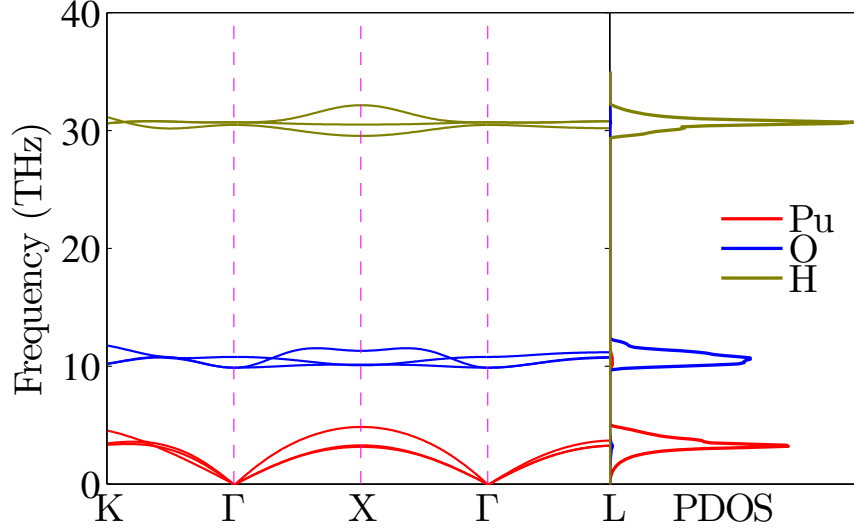


Figure 7: Phonon spectrum (left panel) and phonon DOS (right panel) for $F\bar{4}3m$ -PuO₂ with the LDA+ U fromalium.

O, and H atoms, Pu atoms contribute the lowest acoustic phonon bands (0-5 THz), followed by O atoms (9-12 THz), and finally H atoms (29-32 THz).

275 The thermodynamical quantities at the equilibrium volume $V = V_0$ could be calculated directly by using the above phonon frequencies, while the determination of the quantities at constant pressure P should be combined within the quasiharmonic approximations in which the harmonic approximation holds for every value of V . Now The calculated phonon frequency $\omega_{\nu,\mathbf{q}}(V)$ not only
 280 depends on the band index ν and the Bloch wave vector \mathbf{q} , but also depends on the cell volume V . For specific phonon distribution $\{n_{\nu,\mathbf{q}}\}$, the lattice vibration energy is expressed by $E_{\{n_{\nu,\mathbf{q}}\}}(V) = \sum_{\nu,\mathbf{q}} \hbar\omega_{\nu,\mathbf{q}}(V)(n_{\nu,\mathbf{q}} + 1/2)$, and then the corresponding partition function is given by

$$Z(V, T) = \sum_{\{n_{\nu,\mathbf{q}}\}} \exp(-\beta E_{\{n_{\nu,\mathbf{q}}\}}(V)) = \prod_{\nu,\mathbf{q}} \frac{e^{-\beta\hbar\omega_{\nu,\mathbf{q}}(V)/2}}{1 - e^{-\beta\hbar\omega_{\nu,\mathbf{q}}(V)}}, \quad (10)$$

in which $\beta = 1/(k_B T)$. Using this partition function, we could calculate the
 285 Helmholtz free energy, $F(V, T) = E(V) - k_B T \ln Z(V, T)$ in which $E(V)$ is the in-

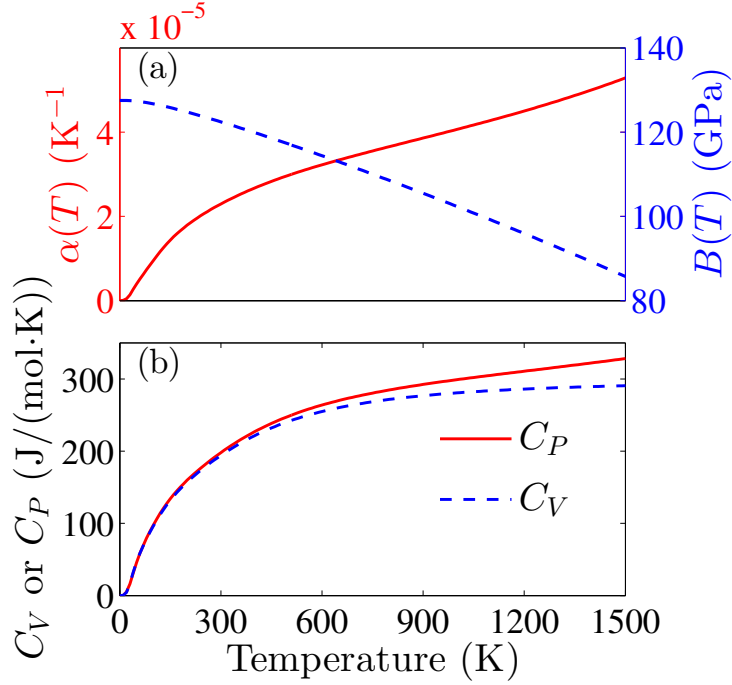


Figure 8: (a) The thermal expansion coefficients $\alpha(T)$ and bulk modulus $B(T)$, and (b) the specific heat C_V and C_P versus the temperature T .

ternal energy as a function of V , and the specific heat at constant volume, $C_V = T \left(\frac{\partial^2 F}{\partial T^2} \right)_V$. Within the quasiharmonic approximation, the Gibbs free energy as a function of P and T could be determined as $G(P, T) = \min_V [F(V, T) + PV]$, and then the specific heat at constant pressure is given by

$$C_P = T \left(\frac{\partial^2 G}{\partial T^2} \right)_P = C_V + VT\alpha^2(T)B(T), \quad (11)$$

290 where the thermal expansion coefficients $\alpha(T)$ and bulk modulus $B(T)$ are given by $\alpha(T) = \frac{1}{V} \left(\frac{\partial V}{\partial T} \right)_P$ and $B(T) = -V \left(\frac{\partial P}{\partial V} \right)_T$, respectively.

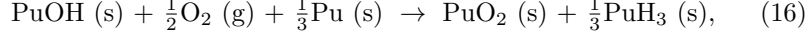
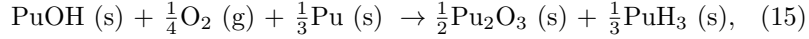
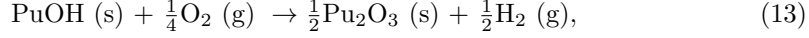
In Figure 8 (a) we plot the thermal expansion coefficients $\alpha(T)$ and bulk modulus $B(T)$ as a function of T . With increasing temperature, the thermal expansion coefficients increase rapidly up to ~ 300 K, and then become slower.
 295 And the bulk modulus decreases approximately linearly as the temperature is

increased. In Figure 8 (b) we plot the specific heat at constant volume and constant temperature of PuOH as a function of temperature. At low temperature, C_V equals to C_P , while at high temperature, C_P keeps positive slope while C_V saturates.

300 At last, we also compute the formation energies E_f^{PuOH} with respect to δ -Pu, molecular hydrogen and oxygen, which is written as as follows:

$$E_f^{\text{PuOH}} = E_{\text{tot}}^{\text{PuOH}} - E_{\text{tot}}^{\text{Pu}} - \frac{1}{2}E_{\text{tot}}^{\text{O}_2} - \frac{1}{2}E_{\text{tot}}^{\text{H}_2}, \quad (12)$$

with $E_{\text{tot}}^{\text{PuOH}}$, $E_{\text{tot}}^{\text{Pu}}$, $E_{\text{tot}}^{\text{O}_2}$, and $E_{\text{tot}}^{\text{H}_2}$ being the total energies of PuOH, δ -Pu, molecular oxygen and hydrogen, respectively. The energies of reaction for the oxidation of PuOH and PuOH-coated Pu metal,



305 are also written as

$$E_r^{\text{PuOH} \rightarrow \text{Pu}_2\text{O}_3} = \frac{1}{2}E_{\text{tot}}^{\text{Pu}_2\text{O}_3} + \frac{1}{2}E_{\text{tot}}^{\text{H}_2} - E_{\text{tot}}^{\text{PuOH}} - \frac{1}{4}E_{\text{tot}}^{\text{O}_2}, \quad (17)$$

$$E_r^{\text{PuOH} \rightarrow \text{PuO}_2} = E_{\text{tot}}^{\text{PuO}_2} + \frac{1}{2}E_{\text{tot}}^{\text{H}_2} - E_{\text{tot}}^{\text{PuOH}} - \frac{3}{4}E_{\text{tot}}^{\text{O}_2}, \quad (18)$$

$$E_r^{\text{PuOH} + \text{Pu} \rightarrow \text{Pu}_2\text{O}_3} = \frac{1}{2}E_{\text{tot}}^{\text{Pu}_2\text{O}_3} + \frac{1}{3}E_{\text{tot}}^{\text{PuH}_3} - E_{\text{tot}}^{\text{PuOH}} - \frac{1}{4}E_{\text{tot}}^{\text{O}_2} - \frac{1}{3}E_{\text{tot}}^{\text{Pu}}, \quad (19)$$

$$E_r^{\text{PuOH} + \text{Pu} \rightarrow \text{PuO}_2} = E_{\text{tot}}^{\text{PuO}_2} + \frac{1}{3}E_{\text{tot}}^{\text{PuH}_3} - E_{\text{tot}}^{\text{PuOH}} - \frac{1}{2}E_{\text{tot}}^{\text{O}_2} - \frac{1}{3}E_{\text{tot}}^{\text{Pu}}. \quad (20)$$

Here $E_{\text{tot}}^{\text{Pu}_2\text{O}_3}$, $E_{\text{tot}}^{\text{PuO}_2}$ and $E_{\text{tot}}^{\text{PuH}_3}$ are the total energies of α -Pu₂O₃, PuO₂, and fcc-PuH₃ compounds, respectively. In Table 3, we list these results and also the experimental values for comparison.

Within LDA, formation energy deviates from the experiment by 2% while
 310 for the LDA+*U* calculation, the difference increase up to 7%. For the GGA calculation, E_f^{PuOH} deviates from the experiment by 4% while within GGA+*U*, the difference decrease to 3%. The larger formation energies found in LDA with respect to GGA are coherent with the overbinding usually found in the LDA

Table 3: Formation energies of PuOH and reaction energies for the oxidation of PuOH and PuOH+Pu for LDA/GGA and LDA/GGA+ U . The experimental values are shown for comparison. All the energies are in units of eV per PuOH formula unit.

	LDA	GGA	LDA+ U	GGA+ U	Exp. [17]
E_f^{PuOH}	-6.71	-6.30	-7.04	-6.34	-6.55
$E_r^{\text{PuOH} \rightarrow \text{Pu}_2\text{O}_3}$	-1.92	-1.89	-2.01	-1.97	-2.04
$E_r^{\text{PuOH} \rightarrow \text{PuO}_2}$	-5.79	-5.05	-5.69	-4.90	-5.46
$E_r^{\text{PuOH}+\text{Pu} \rightarrow \text{Pu}_2\text{O}_3}$	-2.68	-2.54	-2.82	-2.53	-2.69
$E_r^{\text{PuOH}+\text{Pu} \rightarrow \text{PuO}_2}$	-5.10	-4.44	-5.06	-4.20	-4.81

approximation. For the same reason, the reaction of oxidation of PuOH and
 315 PuOH+Pu is more exothermic in LDA(+ U) than in GGA(+ U). All these differences are reasonable and therefore we deduce that our calculation are reliable and consistent.

4. Summary

In this work, we systematically investigate the structural, mechanical, elec-
 320 tronic, optical and thermodynamical properties of PuOH within the framework of density functional theory. The strong local correlation of f electrons in this compound is taken into account by employing the DFT+ U scheme. Firstly, the crystal structure of PuOH, which is experimentally ambiguous, is identified by the total energy calculation. PuOH is predicted to have space group $F\bar{4}3m$
 325 (No. 216). Then the structural properties of $F\bar{4}3m$ -PuOH are calculated and the lattice parameters within the LDA+ U formalism is in good agreement with the experimental value. The mechanical properties such as elastic constants, elastic moduli and Debye's temperature are also computed.

Furthermore, the electronic structures of PuOH are analyzed to reveal the
 330 bonding character. It is found that there is a stronger Pu-O bond and a weaker Pu-H bond. Bader's charge analysis illustrate the Pu(III) cationic feature, which agrees with the experimental arguments. The optical properties of PuOH in-

cluding the reflectivity and absorption coefficient are calculated and might be useful to the contactless identification of this compound.

³³⁵ In the last part, the thermodynamical properties of PuOH are presented. Firstly the phonon spectrum and density of states are given and confirm the dynamical stability of $F\bar{4}3m$ -PuOH. Then some thermodynamical quantities such as the specific heat are presented. The formation energy of PuOH and the reaction energies for the oxidation of PuOH and PuOH+Pu are calculated. The
³⁴⁰ results are in reasonable agreement with the experimental values.

Acknowledgement

We thank Bo Sun and Yongbin Zhang for useful discussions about α -Pu₂O₃. This work was supported by the NSFC (Grant Nos. 11404299, 11305147, and 21471137), the ITER project (No. 2014GB111006), the National 863 Program
³⁴⁵ (No. SQ2015AA0100069), the Science Challenge Program, the Discipline Development Fund Project (No. ZDXKFZ201206), the Foundation of President of CAEP (Nos. 2014-1-58 and 2015-2-12), and the Foundation for Development of Science and Technology of CAEP (Grant No. 9090707).

References

350 **References**

- [1] J. M. Haschke, T. H. Allen, L. A. Morales, Reaction of plutonium dioxide with water: Formation and properties of PuO_{2+x} , *Science* 287 (2000) 285–287.
- [2] J. M. Haschke, T. H. Allen, L. A. Morales, Surface and corrosion chemistry of plutonium, *Los Alamos Science* 26 (2000) 253.
- 355 [3] M. Butterfield, T. Durakiewicz, E. Guziewicz, J. Joyce, A. Arko, K. Graham, D. Moore, L. Morales, Photoemission of surface oxides and hydrides of delta plutonium, *Surface Science* 571 (2004) 74 – 82.
- [4] J. M. Haschke, T. H. Allen, Plutonium hydride, sesquioxide and monoxide monohydride: pyrophoricity and catalysis of plutonium corrosion, *Journal of Alloys and Compounds* 320 (2001) 58 – 71.
- 360 [5] J. Wang, A. K. Ray, A first principles study of water adsorption on α -Pu (0 2 0) surface, *Journal of Nuclear Materials* 424 (2012) 138 – 145.
- [6] A. J. Nelson, P. Roussel, Low temperature oxidation of plutonium, *Journal of Vacuum Science & Technology A* 31 (2013) 031406.
- 365 [7] A. J. Nelson, W. K. Grant, J. A. Stanford, W. J. Siekhaus, P. G. Allen, W. McLean, X-ray excited auger transitions of Pu compounds, *Journal of Vacuum Science & Technology A* 33 (2015) 031401.
- [8] M. N. Huda, A. K. Ray, Molecular hydrogen adsorption and dissociation on the plutonium (111) surface, *Phys. Rev. B* 72 (2005) 085101.
- 370 [9] C. D. Taylor, M. F. Francis, D. S. Schwartz, Thermodynamics, structure, and charge state of hydrogen-vacancy complexes in δ -plutonium, *Phys. Rev. B* 89 (2014) 214114.

- [10] P. Cunningham, J. Haschke, J. Martz, Plutonium storage: Requirements
375 and challenges, Transactions of the American Nuclear Society 69 (1993)
14–18.
- [11] I. Hodges, J. M. Haschke, Corrosion of delta plutonium by synthetic sea
water, Tech. Rep. RFP-2919, Rocky Flats (1979).
- [12] I. Hodges, J. J. Reynolds, J. M. Haschke, Corrosion of delta plutonium in
380 rocky flats tap water, Tech. Rep. RFP-2891, Rocky Flats (1979).
- [13] J. M. Haschke, I. Angela E. Hodges, G. E. Bixby, R. L. Lucas, Reaction
of plutonium with water kinetic and equilibrium behavior of binary and
ternary phases in the Pu + O + H system, Tech. Rep. RFP-3416, Rocky
Flats (1983).
- 385 [14] J. Haschke, A. E. H. III, G. E. Bixby, R. L. Lucas, The reaction of plutonium
with water: phases in the Pu + O + H system, Inorganica Chimica Acta
94 (1984) 122 – 123.
- [15] J. M. Haschke, Hydrolysis of Plutonium: The Plutonium Oxygen Phase
Diagram, American Chemical Society, Washington DC, 1992, Ch. 40, pp.
390 416–425.
- [16] J. Haschke, Reactions of plutonium and uranium with water: Kinetics
and potential hazards, Tech. Rep. LA-13069-MS, Los Alamos National Lab
(1995).
- [17] T. Allen, J. Haschke, Hydride-catalyzed corrosion of plutonium by air:
395 Initiation by plutonium monoxide monohydride, Tech. Rep. LA-13462-MS,
Los Alamos National Lab (1998).
- [18] J. Haschke, T. Allen, L. Morales, D. Jarboe, C. Puglisi, Chloride-catalyzed
corrosion of plutonium in glovebox atmospheres, Tech. Rep. LA-13428-MS,
Los Alamos National Lab (1998).

- 400 [19] A. B. Shick, V. Drchal, L. Havela, Coulomb- U and magnetic-moment collapse in δ -Pu, *Europhysics Letters* 69 (2005) 588.
- [20] B. Sun, P. Zhang, X.-G. Zhao, First-principles local density approximation + U and generalized gradient approximation+ U study of plutonium oxides, *The Journal of Chemical Physics* 128 (2008) 084705.
- 405 [21] G. Jomard, B. Amadon, F. Bottin, M. Torrent, Structural, thermodynamic, and electronic properties of plutonium oxides from first principles, *Phys. Rev. B* 78 (2008) 075125.
- [22] P. Zhang, B.-T. Wang, X.-G. Zhao, Ground-state properties and high-pressure behavior of plutonium dioxide: Density functional theory calculations, *Phys. Rev. B* 82 (2010) 144110.
- 410 [23] B. Sun, H. Liu, H. Song, G. Zhang, H. Zheng, X. Zhao, P. Zhang, The environmental dependence of redox energetics of PuO_2 and $\alpha\text{-Pu}_2\text{O}_3$: A quantitative solution from DFT+ U , *Physics Letters A* 376 (2012) 2672 – 2676.
- 415 [24] B.-Y. Ao, J.-J. Ai, T. Gao, X.-L. Wang, P. Shi, P.-H. Chen, X.-Q. Ye, Metal-insulator transition of plutonium hydrides: DFT+ U calculations in the FPLAPW basis, *Chinese Physics Letters* 29 (2012) 017102.
- [25] B. Ao, X. Wang, P. Shi, P. Chen, X. Ye, X. Lai, T. Gao, First-principles LDA+ U calculations investigating the lattice contraction of face-centered cubic pu hydrides, *Journal of Nuclear Materials* 424 (2012) 183 – 189.
- 420 [26] B.-Y. Ao, P. Shi, Y. Guo, T. Gao, Abnormal lattice contraction of plutonium hydrides studied by first-principles calculations, *Chinese Physics B* 22 (2013) 37103.
- [27] G. Yong, A. Juan-Juan, G. Tao, A. Bing-Yun, Structural, magnetic, electronic, and elastic properties of face-centered cubic PuH_x ($x=2,3$): GGA (LSDA) + U + SO, *Chinese Physics B* 22 (2013) 057103.
- 425

- [28] J.-J. Zheng, B.-T. Wang, I. D. Marco, W.-D. Li, Electronic structure and phase stability of plutonium hydrides: Role of coulomb repulsion and spin-orbital coupling, *International Journal of Hydrogen Energy* 39 (2014) 13255 – 13265.
- 430 [29] Y. Yang, P. Zhang, Hydriding and dehydriding energies of PuH_x from ab initio calculations, *Physics Letters A* 379 (2015) 1649 – 1653.
- [30] G. Kresse, J. Furthmüller, Efficient iterative schemes for *ab initio* total-energy calculations using a plane-wave basis set, *Phys. Rev. B* 54 (1996) 11169–11186.
- 435 [31] P. E. Blöchl, Projector augmented-wave method, *Phys. Rev. B* 50 (1994) 17953–17979.
- [32] G. Kresse, D. Joubert, From ultrasoft pseudopotentials to the projector augmented-wave method, *Phys. Rev. B* 59 (1999) 1758–1775.
- 440 [33] J. P. Perdew, A. Zunger, Self-interaction correction to density-functional approximations for many-electron systems, *Phys. Rev. B* 23 (1981) 5048–5079.
- [34] J. P. Perdew, K. Burke, M. Ernzerhof, Generalized gradient approximation made simple, *Phys. Rev. Lett.* 77 (1996) 3865–3868.
- 445 [35] H. J. Monkhorst, J. D. Pack, Special points for brillouin-zone integrations, *Phys. Rev. B* 13 (1976) 5188–5192.
- [36] A. I. Liechtenstein, V. I. Anisimov, J. Zaanen, Density-functional theory and strong interactions: Orbital ordering in mott-hubbard insulators, *Phys. Rev. B* 52 (1995) R5467–R5470.
- 450 [37] H. Y. Geng, Y. Chen, Y. Kaneta, M. Kinoshita, Q. Wu, Interplay of defect cluster and the stability of xenon in uranium dioxide from density functional calculations, *Phys. Rev. B* 82 (2010) 094106.

- [38] F. Birch, Finite elastic strain of cubic crystals, *Phys. Rev.* 71 (1947) 809–824.
- 455 [39] Y. Le Page, P. Saxe, Symmetry-general least-squares extraction of elastic data for strained materials from *ab initio* calculations of stress, *Phys. Rev. B* 65 (2002) 104104.
- [40] R. Hill, The elastic behaviour of a crystalline aggregate, *Proceedings of the Physical Society. Section A* 65 (1952) 349.
- 460 [41] W. Voigt, *Lehrbuch der Kristallphysik*, Teubner, Leipzig, 1928.
- [42] A. Reuss, *Z. Angew. Math. Mech.* 9 (1929) 49–58.
- [43] P. Debye, Zur theorie der spezifischen wärmen, *Annalen der Physik* 344 (1912) 789–839.
- 465 [44] M. Born, K. Huang, *Dynamical Theory of Crystal Lattice*, Oxford University Press, Oxford, 1954.
- [45] S. C. Abrahams, F. S. L. Hsu, Debye temperatures and cohesive properties, *The Journal of Chemical Physics* 63 (1975) 1162–1165.
- [46] I. D. Prodan, G. E. Scuseria, R. L. Martin, Covalency in the actinide dioxides: Systematic study of the electronic properties using screened hybrid
470 density functional theory, *Phys. Rev. B* 76 (2007) 033101.
- [47] X.-D. Wen, R. L. Martin, L. E. Roy, G. E. Scuseria, S. P. Rudin, E. R. Batista, T. M. McCleskey, B. L. Scott, E. Bauer, J. J. Joyce, T. Durakiewicz, Effect of spin-orbit coupling on the actinide dioxides AnO_2 (An=Th, Pa, U, Np, Pu, and Am): A screened hybrid density functional
475 study, *The Journal of Chemical Physics* 137 (2012) 154707.
- [48] R. F. W. Bader, *Atoms in Molecules: a Quantum Theory*, New York: Oxford University Press, 1990.

- [49] R. Kubo, Statistical-mechanical theory of irreversible processes. i. general
480 theory and simple applications to magnetic and conduction problems, Journal of the Physical Society of Japan 12 (1957) 570–586.
- [50] D. A. Greenwood, The boltzmann equation in the theory of electrical conduction in metals, Proceedings of the Physical Society 71 (1958) 585.
- [51] M. Gajdoš, K. Hummer, G. Kresse, J. Furthmüller, F. Bechstedt, Linear
485 optical properties in the projector-augmented wave methodology, Phys. Rev. B 73 (2006) 045112.
- [52] H. Shi, M. Chu, P. Zhang, Optical properties of UO_2 and PuO_2 , Journal of Nuclear Materials 400 (2010) 151 – 156.
- [53] A. Togo, F. Oba, I. Tanaka, First-principles calculations of the ferroelastic
490 transition between rutile-type and CaCl_2 -type SiO_2 at high pressures, Phys. Rev. B 78 (2008) 134106.